Soil Dynamics and Earthquake Engineering 77 (2015) 299–308

Contents lists available at ScienceDirect

Soil Dynamics and Earthquake Engineering

journal homepage: www.elsevier.com/locate/soildyn

An elastic-wave-based full-wavefield imaging method for investigating defects in a high-speed railway under-track structure

Ailan Che [1], Zheng Tang, Shaokong Feng

School of Naval Architecture, Ocean and Civil Engineering, Shanghai Jiaotong University, 800 Dongchuan-Road, Shanghai, 200240, China

ARTICLE INFO

Article history:
Received 4 November 2014
Received in revised form
31 May 2015
Accepted 11 June 2015

Keywords:
Full-wavefield imaging method
Multi-scale layered media
Wave propagation
Under-track structure of high-speed railway
Full-scaled model test

ABSTRACT

In geotechnical engineering, defect detection for concrete structure can be simplified as a multi-layered media problem in most cases. The types of defects are mainly identified as cracks inside the concrete, interlaminar peeling, and loose bedding voids. The study of the wave propagation phenomenon in multi-scale layered media and the effects on defects merits investigation. The present research focuses first on the analysis of this phenomenon using numerical methods. The wave propagation characteristics of the multi-layered model with defects are assessed with dynamic FEM analyses under three-dimensional conditions. The analysis is obtained in the time domain and allows the consideration of multiple wave reflections between layers. Based on this analysis, a full-wavefield imaging detection method is developed and then applied to reveal the defects in the under-track structure of a high-speed railway. This testing system integrates the point-source/point-receiver scheme with the multi-directional imaging technique to achieve an effect analogous to that achieved with scanning. It is equipped with an impacting hammer, a series of three-component velocity transducers and a signal capturing unit. To evaluate the feasibility of this system for detecting defects in the under-track structure of the high-speed railway, a full-scaled high-speed railway model test with pre-setting defection is conducted. The data are analyzed according to characteristics of waveform and wave energy. The average amplitude is used to evaluate the defect area. It is concluded that the full-wavefield imaging detection method exhibits high potential for inspecting the defects of the under-track structure of high-speed railways by imaging.

© 2015 Elsevier Ltd. All rights reserved.

1. Introduction

High speed railway is experiencing rapid growth in China. It is considered as an important role in technological progress and socioeconomic development, giving the advantages it offers in terms of transportation, energy consumption and environmental pollution [8]. However, it raises more complex engineering problems. Therefore, the entire railway system must be in excellent condition to guarantee traveling safety and comforting at speeds of 200–350 km/h. In this rapidly operating high-speed railway system, the under-track structure (mainly each structural layer under the track and the subgrade) bears directly on the high-speed trains' loading. With faster running speeds, expanding freight volumes and environmental changes, some defects appears in the under-track structure. Data collected on the Sui-Yu railway show that cracks have occurred on the back surface of the track plate [13]. Cracks in the track plate, escaping from the mortar layer and cracking and mud spillover in the support layer are major defects occurring in high-speed railways in China, as shown in Fig. 1. Defects existing in the track substructure will increase the dynamic action between the train and the track and will aggravate the rail vibration, which will gradually generate other damage and weaken the performance of the railway system over time [21]. Therefore, safety regulations and economic strategies may mandate regular inspections or the continuous monitoring of these structures using a non-invasive method.

Non-destructive inspection (NDI) can be visual, optical, magnetic, radiographic, thermographic, nuclear, or elastodynamic [11,20]. The detection of the under-track structure of high-speed railways involves mainly static and dynamic penetration tests, a high-density resistivity method and the Rayleigh wave method for subgrade and GPR for concrete [3]. These techniques have been used in some challenging sections of engineering such as required quantitative evaluations for cracks, loose areas and escape between layers. Recently, the elastic-wave-based techniques have received significant attention in the implementation of nondestructive testing (NDT) technologies for civil engineering. Traditional elastic-wave inspection methods (e.g., pulse-echo, through transmission, and pitch–catch) employ a single point source/point receiver arrangement to recognize a defect from changes in received signals [17], while modern elastic-wave imaging techniques (e.g., the synthetic aperture focusing technique, SAFT)

E-mail address: alche@sjtu.edu.cn (A. Che).
[1] Tel./fax: +86 2134 206 564.

http://dx.doi.org/10.1016/j.soildyn.2015.06.005
0267-7261/© 2015 Elsevier Ltd. All rights reserved.

Fig. 1. Major defects occurred in high-speed railway in China: cracks in the track plate, escape of mortar layer, and cracking and mud spillover in the support layer.

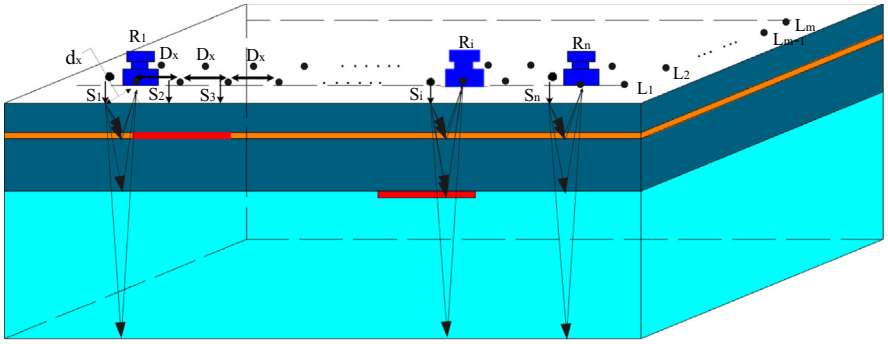

Fig. 2. Schematic showing the implementation of impact-and-receive operations.

employ a multiple source/receiver arrangement to scan a structure with defects [15]. In detecting defects in concrete, an elastic-wave-based imaging method is used to display the tip of surface-breaking cracks [4,22]. The point-source/point-receiver scheme is particularly suitable for the inspection of on-site civil infrastructures. In 2008, Che et al., Feng et al. [5,9] and Liu et al. [14] proposed an elastic-wave imaging method to investigate the grouting construction of immersed tube tunnels. This method could be a practical and effective NDT method for the inspection of defects in civil infrastructures. However, these studies focus on a single scale and a single direction. The image quality can be affected by the reflection of boundaries, since the boundaries of an inspection structure undergo a limited inspection. Therefore, a greater number of signals are captured by inspecting multiple directions, which can thus collect a greater amount of information under the structures.

In the context of elastic-wave NDI, layered structures are collectively known as propagations of elastic waves. The presence of elastic waves with long wavelengths has given elastic-wave inspection methods considerable potential for rapid, long-range examination of layered structures. Dalton et al. [6], for example, have concluded that guided elastic waves possess good sensitivity to localized damage. Rose [19] has supplied an extremely comprehensive account of the state of the art as well as the future vision of NDI with guided elastic waves. In structural health monitoring with elastic waves, a comparison between the measurements of a flawed structure with those of an identical but flawless one is required. Mathematical modeling can be analytical, numerical, or a combination thereof (i.e., semi-analytical) [12,1,7]. Moreover, our fundamental understanding of elastic-wave phenomena is based on these models. However, these models are based on simplifications of geometry and/or boundary conditions. Therefore, they are only applicable to simple cases. The more practical but complex problems can be only addressed using numerical methods. There are several numerical methods to model elastic wave scattering [2,16,10], including the finite element method (FEM), the spectral

finite element method (SFEM), the finite difference method (FDM), and the surface integral method (SIM). The FEM is the most frequently used method in modeling elastic wave propagation and scattering. The different uses of FEM in elastic-wave modeling can be distinguished by using two parent categories: pure and hybrid. The pure usage of FEM can be achieved with numerical implementations or commercial software packages. In this paper, a 3D layered model with a multi-scaled orientation is built and a finite element method is employed to analyze the propagation characteristics of elastic waves in the application of the numerical model. Moreover, a comparison based on physical experiments enables a full-scale model test of a high-speed railway to be conducted.

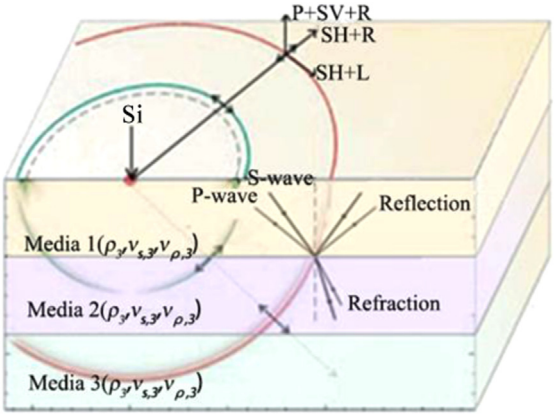

Fig. 3. Propagation of elastic wave in semi-infinite space.

2. Full-wavefield imaging method

2.1. Principles and data collection

To match the present NDT measuring scheme in civil engineering, the measurement of a full-wavefield imaging detection method is managed with a point-source/point-receiver set with a specified space. As shown in Fig. 2, a series of impact-and-receive operations are performed on the free surface of the model. Let Si and Ri represent the locations of a set of the source and receiver for the i-th measurement. Furthermore, let Ti(t) be the response signal recorded at Ri for this measurement. The domain of Ti(t) is then divided into three directions such that the wave characteristic and its spectrum of Ti(t) can be obtained in these three directions.

As we know, in a semi-infinite space, a localized disturbance on the surface of an elastic medium should occur in an oscillated pattern [18]. Loading from any surface point, the type of the wavefield, the displacement mode, the propagation direction and the amplitude can be described, as demonstrated in Fig. 3. Longitudinal waves (P) and shear waves (S=SH+SV) propagate radially outward along the radial direction of the hemispherical centered

Table 1
Mechanical parameters of media in the model.

No.	Physical variable	Density ρ (kg/m^3)	Poisson ratio μ	Dynamic elastic modulus E (GPa)
$V1$	Concrete	2400	0.2	34.5
$V2$	CA mortar	1400	0.168	25
$V3$	Defect	1100	0.45	0.001
$V4$	Embankment (graded broken stone)	2300	0.25	250.5

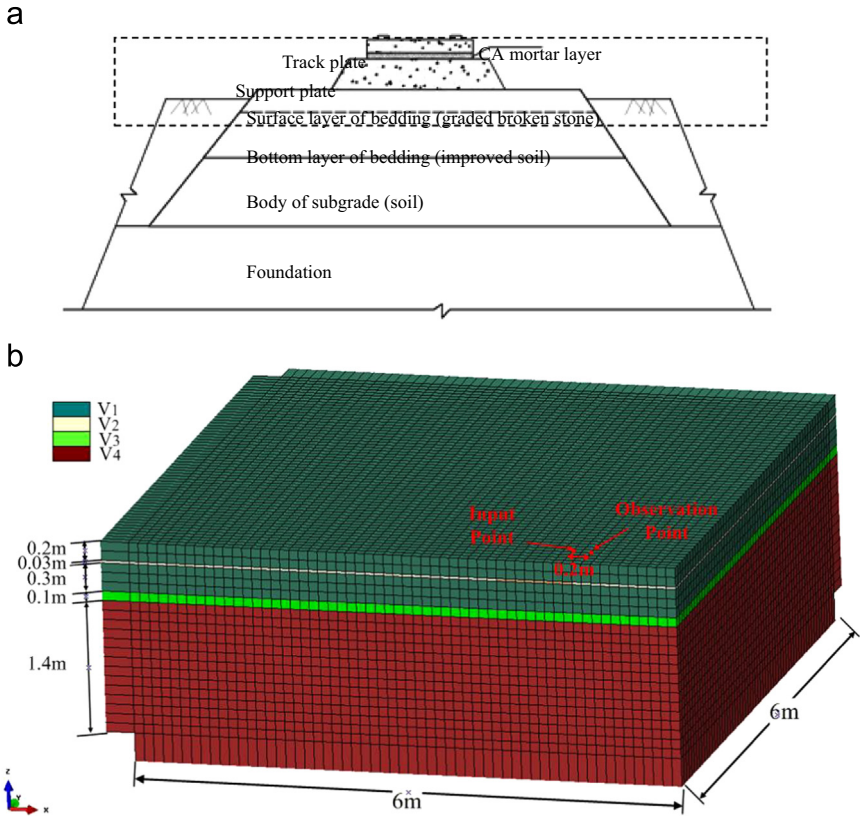

Fig. 4. Multi-layered model: (a) under-track structure of high speed railway and (b) mesh of model.

on the excited point. The wave surface of the Rayleigh wave (R) is a cylindrical surface centered on the excited point as the column center. This wave consists of horizontal and vertical components, which compose an elliptical trajectory. Its amplitude rapidly decreases with the increasing depth of both the vertical and horizontal components. When the medium is a layered structure, other surface waves, known as Love waves (*L*), will arise in the media surface. The propagation direction of a Love wave is perpendicular to the wave propagation and parallel to the surface of the medium. When the materials of the medium are different, reflection and refraction will occur. The response is complicated due to the simultaneous presence of P-waves, S-waves and surface waves as well as converted waves, as shown in Fig. 3.

A full-wavefield imaging method is conducted in the following steps:

1) Add position information: Assign the positions of source and receiver to the seismic data at the beginning of data processing.
2) Normalization with impact strength: Normalize the seismic data with the acceleration recorded by an accelerometer on the hammer to reduce the influence of the variation of impact strength.
3) Create common offset gather: Abstract common offset traces from the field of common source data to create a common offset gather.
4) Noise reduction: The data may present different types of noise. Reduce noise with time windows and band pass filters.
5) Create waveform section: Reorder the traces in the common offset gather according to their position on the survey line to create a *Time–Waveform* section. All further processing will be conducted on this section.
6) Calculate impact response: To evaluate the impact image quantitatively, the average amplitude is calculated as an index called *Impact Response*, with the average amplitude reflecting the response of the media to the impact. The impact response can be represented as a line graph, a contour map, or a color-scaled cloud map.
7) Standardize impact response: In some cases, we expect to use a value with no dimension to evaluate the inspected media. This evaluation can be achieved by constructing a reference line in the area without defects and standardizing the impact response with that of the reference data.
8) Comprehensive evaluation: Based on the numerical results of wave propagation, the final results are determined as a weighted average of the three-directional impact response.

3. Wave propagation in multi-scaled layered media

Most cases of detecting defects in a concrete structure can be simplified as a multi-scaled layer media problem. The under-track structure of high speed railway consists of four layers, which are, from top to bottom, a track plate, a CA mortar layer, a support layer, and the embankment. The embankment includes the surface layer (graded broken stone), bottom layer (improved soil) and body of subgrade, as shown in Fig. 4(a). The subject of the current study is an infinite 3D model with five layers (track plate, a CA mortar layer, support layer, graded broken stone layer and defects layer), with the thickness *h* distributed as thin and thick layers, as shown in Fig. 4(b). The model is described by a rectangular coordinate system (*x*, *y*, *z*). The *x*-axis and *y*-axis constitute the model's infinite dimension. The model is assumed to be symmetrical about the *y*–*z* and the *x*–*z* planes; therefore, only 1/4 of the model is shown. Because information about propagating in the unloaded model is required to determine whether adequate FE discretization has occurred, free elastic waves in the infinite width models will be handled later.

Numerical methods are used in the field of elastic wave modeling: 1) FEM dynamic analyses are performed to describe the wave propagation; 2) a Ricker wavelet is used as the impulsive response, which is characterized by a simple function excitation force and concentrated in a short time duration of action; and 3) the response of elastic waves with 5 types of models are discussed. As shown in Fig. 4, *V*1, *V*2, *V*3 and *V*4 signify the physical parameters (including density, elastic modulus and Poisson ratio) of material 1, 2, 3 and 4, respectively. A medium can be a homogenous half-space. If $V1=V2=V3=V4$, then the media constitute concrete slabs on a homogenous half-space with no defects. If $V1 \neq V2 \neq V3 \neq V4$, a model can be considered to be multi-layered. If $V2$, $V3 \approx 0$, the model can be considered to be a void under a concrete slab or between concrete slabs. For the strength

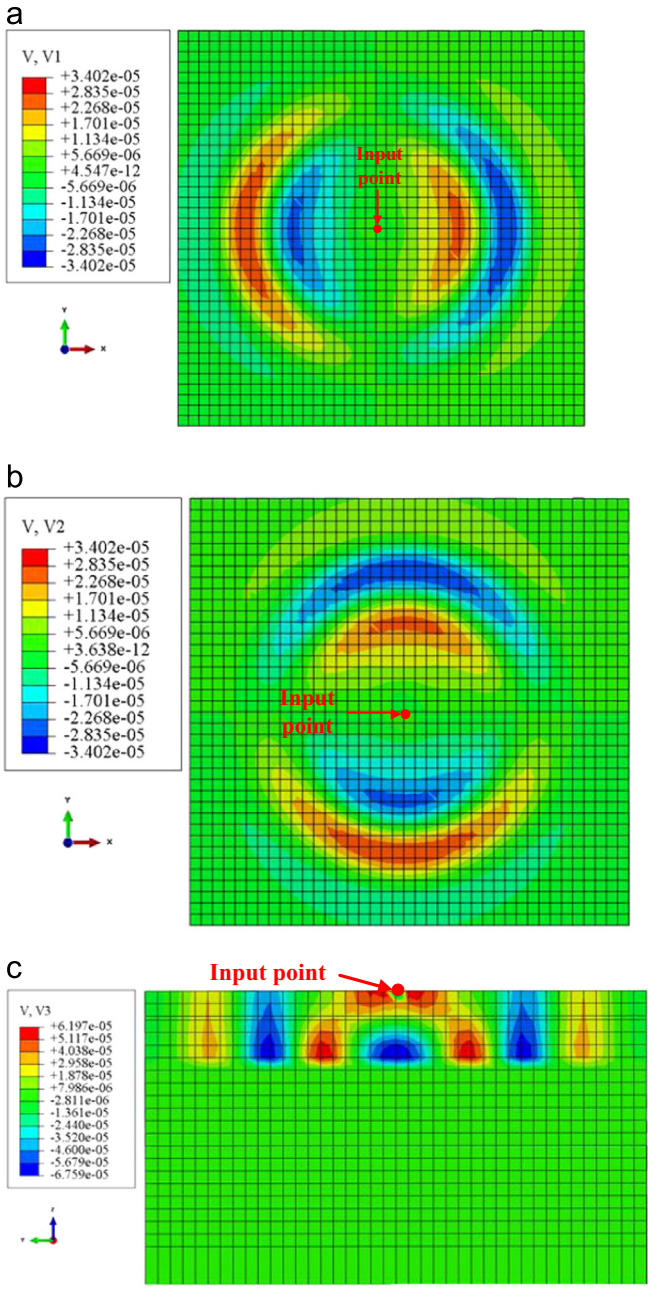

Fig. 5. Distributions of horizontal and vertical velocity (case 3, $t=0.010264$ s): (a) in *x* direction, (b) in *y* direction, and (c) in *z* direction.

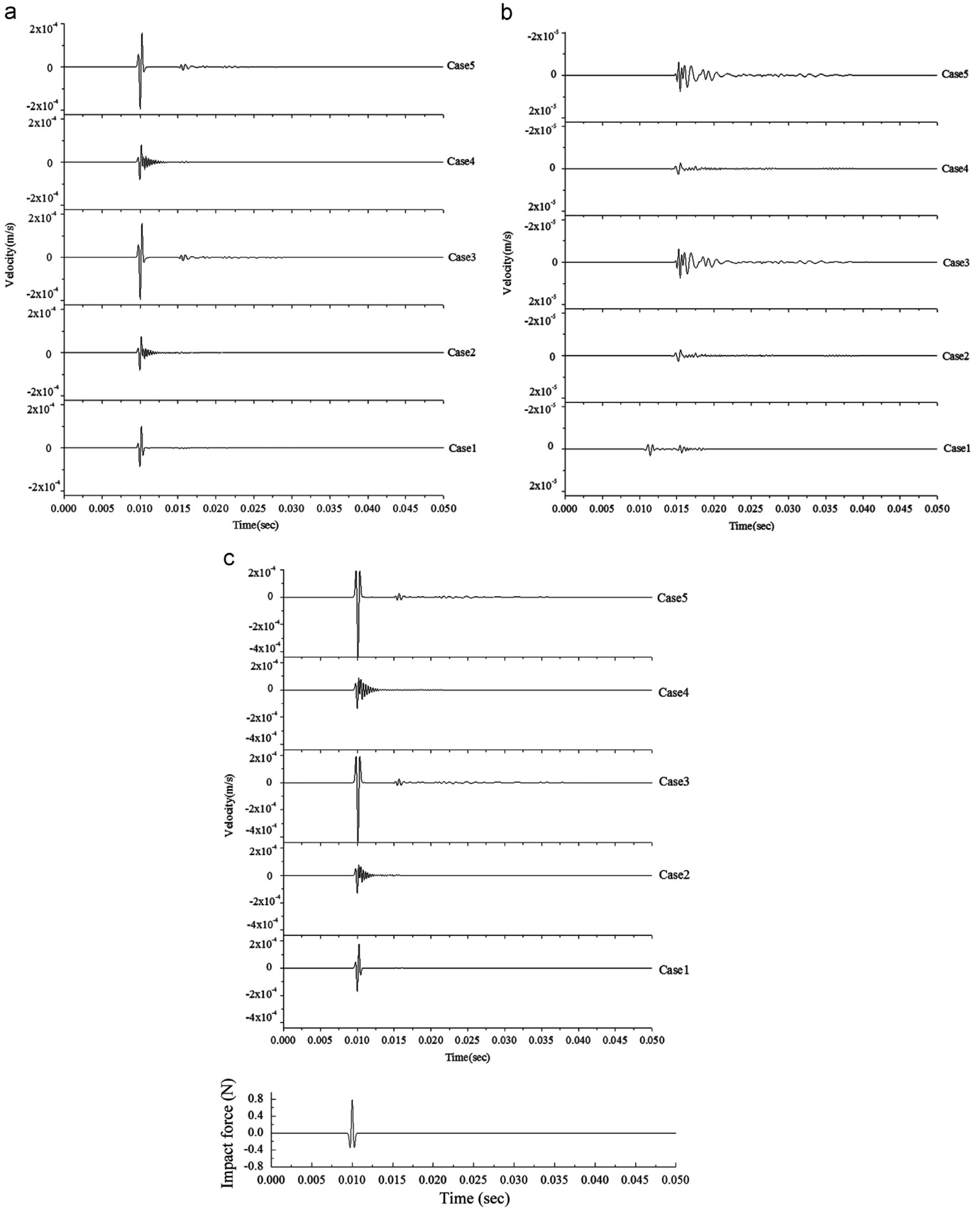

Fig. 6. Distribution of waveform: (a) in *x* direction, (b) in *y* direction, and (c) in *z* direction.

of the wave observed at the surface of the model depends on the reflection coefficient of interface between layers, the defects also are simulated as layered where the influence of its depth is ignored.

The material parameters are chosen from the conditions modeled on real conditions. All of the material parameters are listed in Table 1, while ρ is the density of material, E is the modulus, and μ is Poisson's ratio. A Ricker wavelet is assumed to be impacted at the surface of the model with a frequency of $f=1500$ Hz, $t=0.05$ s, while $\Delta t=1.0\times10^{-5}$ s and is the unit amplitude, which is used as the time-dependent force in the vertical direction.

A series of impact-and-receive operations are performed on the top surface of the model, as shown in Fig. 4. The response signals of the velocity recorded by the nearby receiver on the surface are obtained from further processing. By inputting the vibration source on the surface in the center of the model, the dynamic response can be obtained. Five types of models are tested, which correspond to the following five cases: case 1: $V1=V2=V3=V4$; case 2: $V1\neq V2\neq V3=V4$; case 3: $V2\approx 0$; case 4: $V3\approx 0$; and case 5: $V2$, $V3\approx 0$.

Fig. 5 shows the distribution of the horizontal and vertical velocities of the model at time 0.010264 s, when the color is changed by the amplitude. The figure also shows the form of the surface wave propagation and indicates that reflection and refraction have occurred on the surface of the CA mortar layer. Fig. 6 shows the horizontal and vertical velocities of the waveform at the receiver. The responses in the x and z directions are similar to the Rayleigh wave, which plays a dominant role. The response in the y direction is remarkably different, resulting in a value that is smaller by a number of orders because of the Love wave effect. When $Vi\approx 0$, a strong reflection and refraction will occur on the surface, and the energy of the waveform will increase. Fig. 7 shows the average amplitude of the velocity response for the five models. The impact response appears most in the z direction, followed by the x direction, and the response in the y direction is approximately 1/10 that of the x direction. Compared with different models, the impact response increases the number of defects in

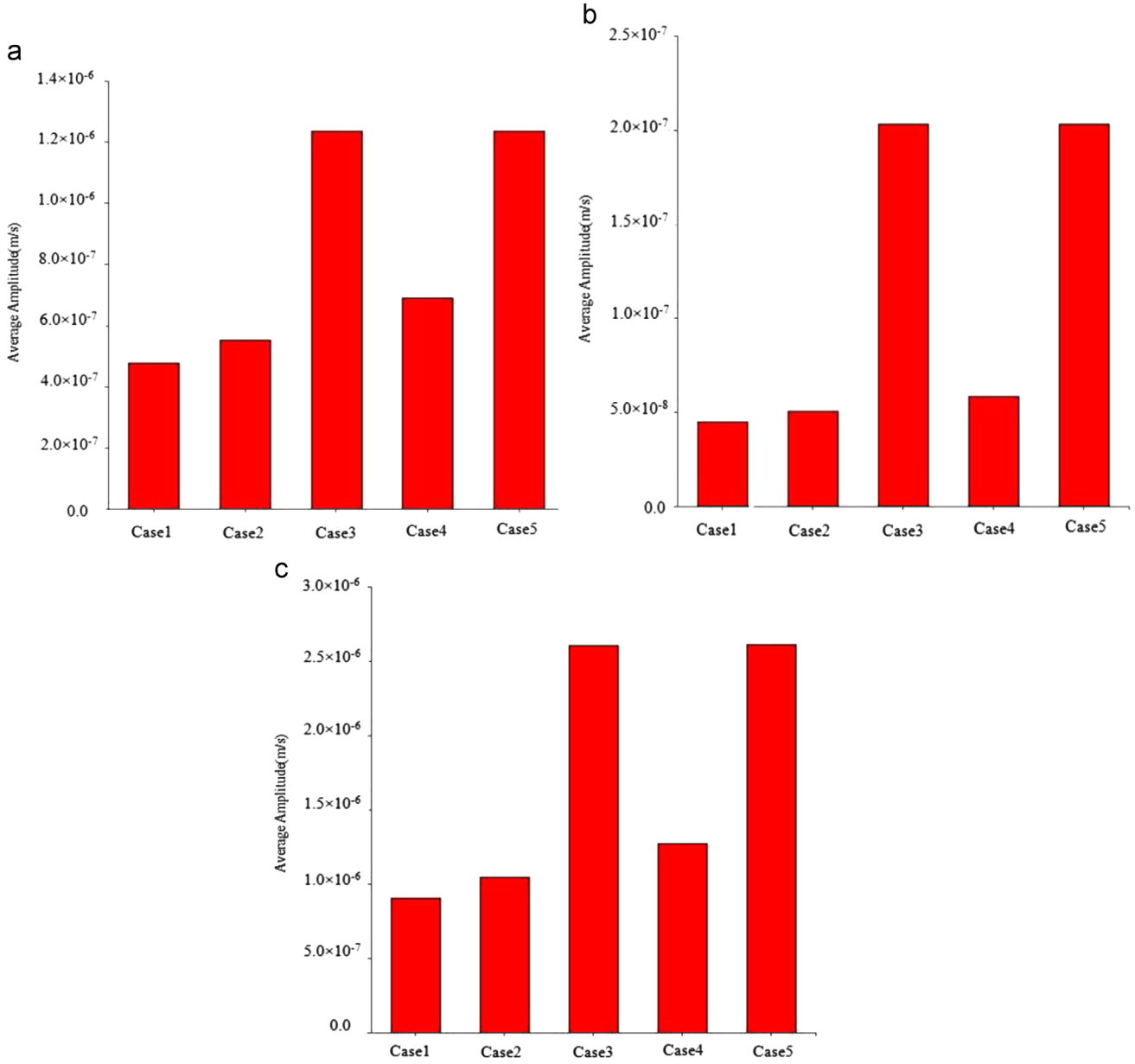

Fig. 7. Distribution of impact response: (a) in x direction, (b) in y direction, and (c) in z direction.

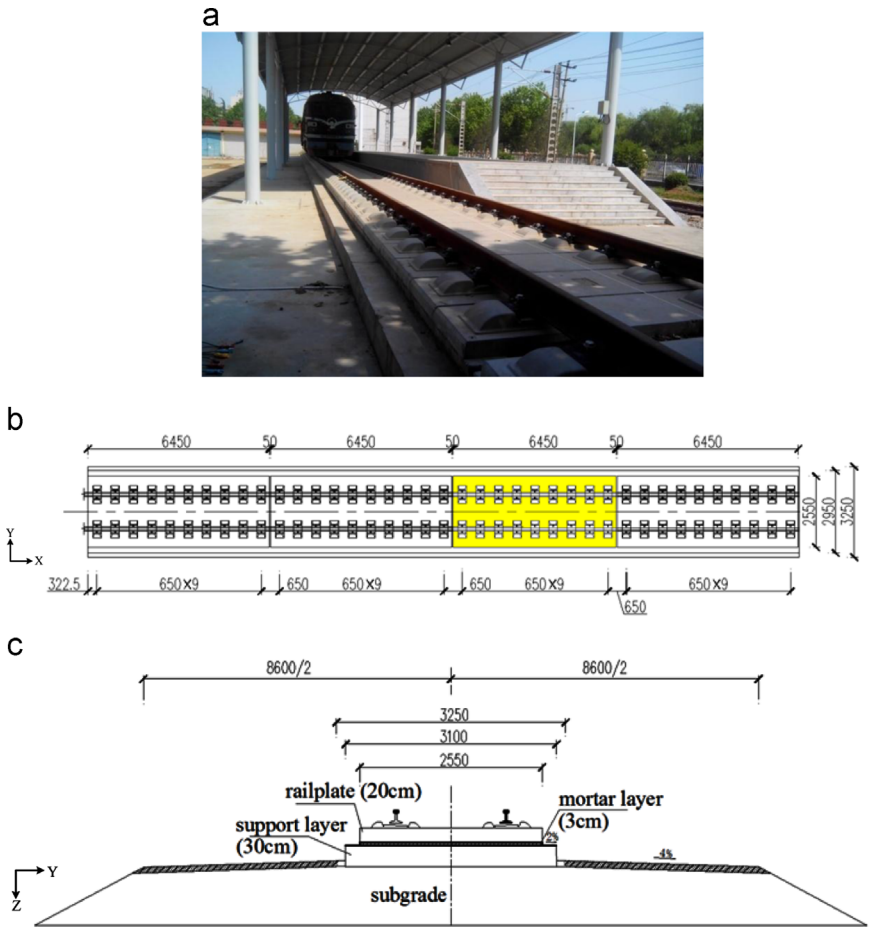

Fig. 8. Overview of model: (a) photograph of site model, (b) plane view, and (c) cross section.

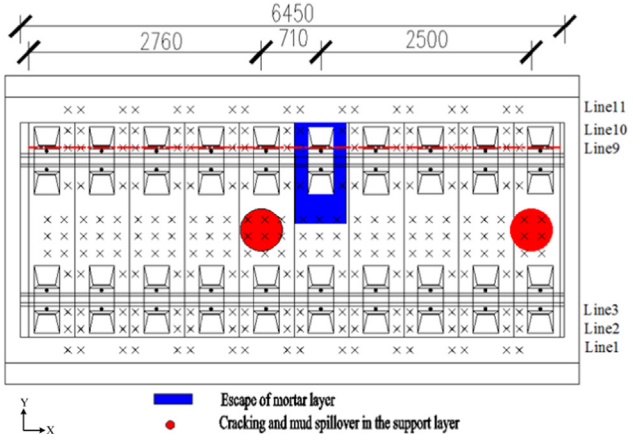

Fig. 9. Defect constructions.

Fig. 10. Data acquisition.

the *x* direction by 2.25 times in case 3 and case 5 and 1.25 times in case 4; in the *y* direction, by 4.0 times in case 3 and case 5 and 1.15 times in case 4; and in the *z* direction, 2.5 times by defects in case 3 and case 5 and 1.22 times in case 4.

4. Model test of a high-speed railway

4.1. Test introduction

To evaluate the feasibility of the observation system, a model test is conducted at Shijiazhuang Railway University, China. The model is built with the materials and methods appropriate for constructing high-speed rail, as shown in Fig. 8(a). Referring to the CRTS II type ballastless track standard structure of high-speed rails in China, a full-scale model is constructed. It measures 26.2 m in length and 3.65 m in width and consists of four panels, each 6.45-m long, as shown in Fig. 8(b), with the third panel constructed to contain a series of defects. The structure consists of four layers, which are, from top to bottom, a track plate, a CA mortar layer, a

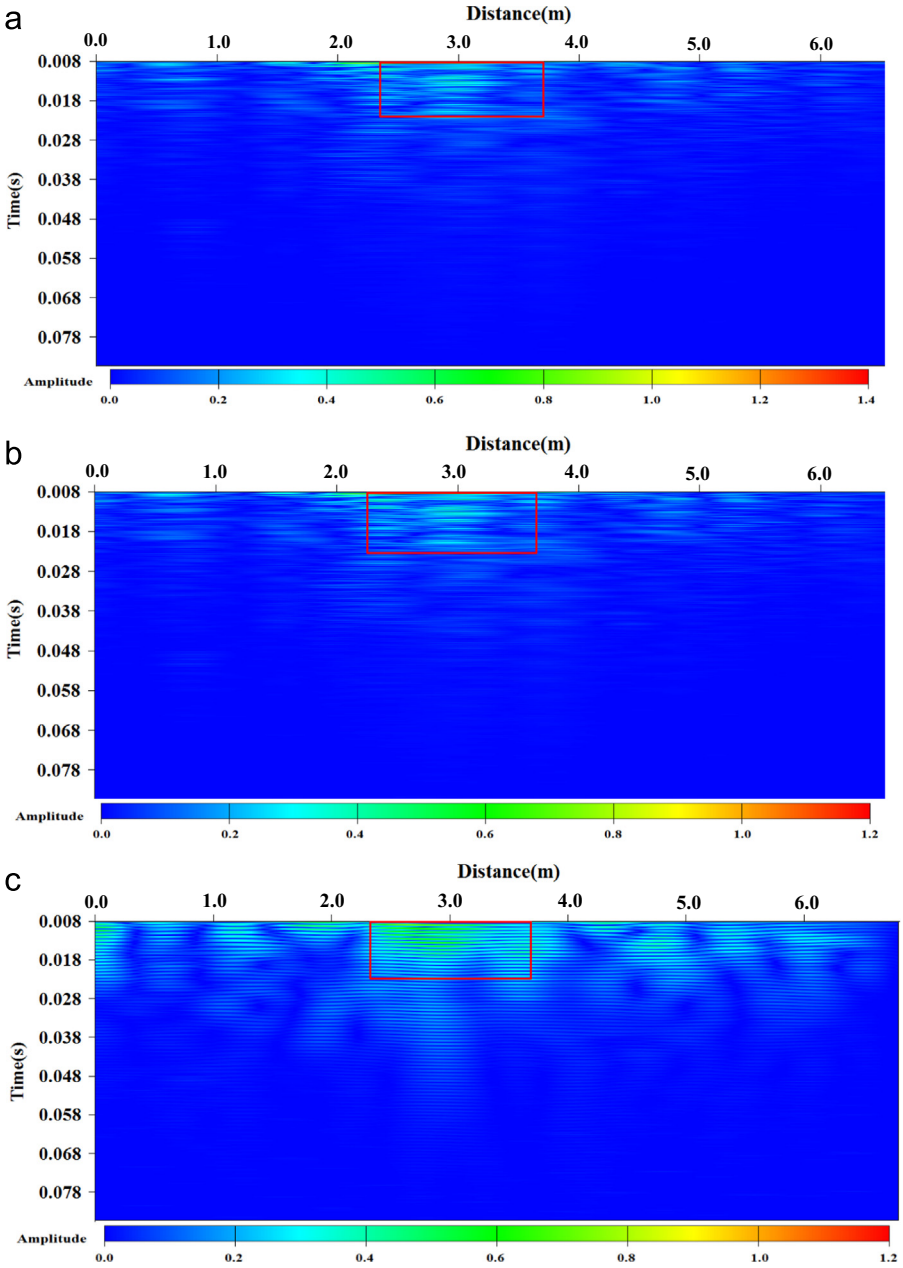

Fig. 11. Impact image of survey line 9, (a) in *x* direction, (b) in *y* direction, (c) in *z* direction.

support layer, and the embankment. The dimensions of the first three layers are 2.55 m × 0.20 m, 2.55 m × 0.05 m, and 3.15 m × 0.30 m. The embankment is trapezoidal, with a thickness of 0.60 m and a gradient of 1:1, as shown in Fig. 8(c).

According to the statistical incidence of major defects in high-speed railways in China, escape of the CA mortar layer is widely occurred in CRTS II type of ballastless track and massive mud spillover from the top of embankment is occurred in CRTS I of ballastless track. Those damages cause cracks in the track and support plate. Through visual and simple measurements, the void between CA mortar layer and track plate is 1–5 mm depth, and there are also exists loose area in the CA mortar layer. According to the grouting volume under support plate, there possibility forms cavities less than 20 mm depth at the top of embankment. In the model tests, two types of defects are pre-constructed in the model, as shown in Fig. 9. The area and depth of defects are amplified to verify the detection method and it is convenient to product. These defects are constructed by the following methods: (1) escape of the mortar layer created by scratching a 0.60 m × 1.00 m defect in the CA mortar layer; and (2) cracking and mud spillover in the support layer created by digging a hole of 0.5 m in diameter and 0.25 m deep at the top of the embankment and then burying it loosely with soil.

4.2. Data collection

This testing system is equipped with an impacting hammer, a series of three-component velocity transducers and a signal capturing unit, as shown in Fig. 10. A digital seismo-graph (Geode) with a 24-channel (Ch) and a 24-bit A/D conversion is used to collect data. The 3-component geophones with 2-horizontal and 1-vertical directions on the pavement and a coupling device are used for receiving the ground response motivated by a 50-g metal hammer. The interval of receivers is set to be 0.2 m and the space between survey lines is initialized to be 0.2 m. The source offset is 0.2 m, and the survey area is divided into 0.2 m × 0.2 m meshes, as

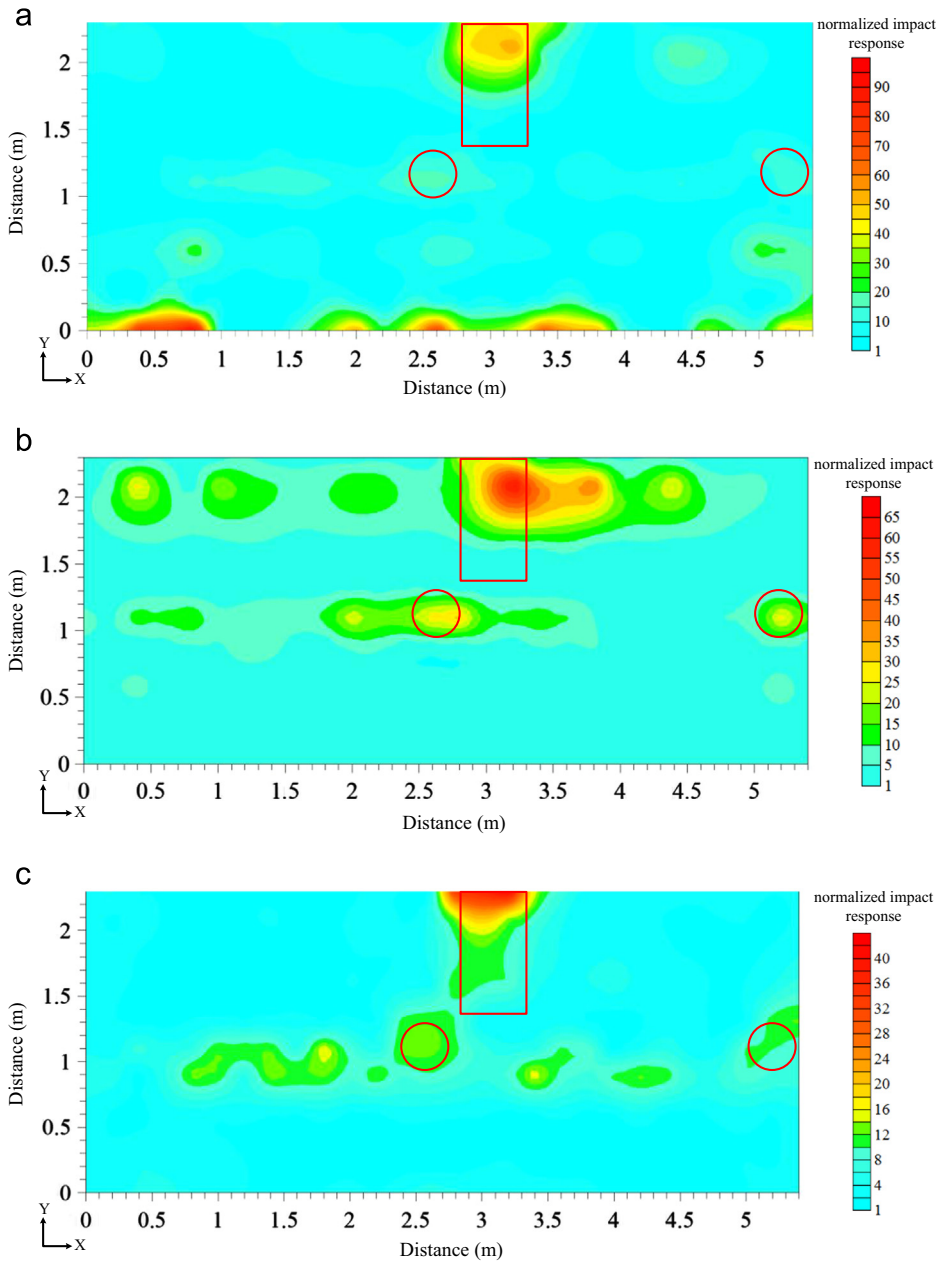

Fig. 12. Distribution of normalized impact response, (a) in *x* direction, (b) in *y* direction, (c) in *z* direction.

shown in Fig. 9. To complete the survey efficiently and methodically, 4 receivers are arranged in a survey line, and 4 source points (impact points) are set: for each impact, 4 different offset data will be obtained for each line, though only one offset is used in the analysis. To guarantee the test accuracy, three-component velocity transducers are set as stable as possible, and the impact strength keeps as the same. It needs the test surface keep as smooth as possible, and there are no strong noise surrounding the test area.

4.3. Data analysis and results

The experiment is then conducted with a series of impact-and-receive operations on the top surface of the concrete plate. The diagram of the velocity waves is constructed when the concrete plate is impacted by a hammer. All the data are processed in the same sequence with the same parameters.

Fig. 11 shows the seismic impact image in three directions as an example. It is clear that the duration of the seismic wave at the defect area becomes longer and the intensity increases. According to the discussion before, the seismic data recorded at the surface of a concrete slab can be represented as the summation of multiples. Because the density and the wave velocity of the defect are significantly smaller than those of the concrete, the reflection coefficient is smaller in the no defect area. Thus, the seismic wave appeals to be stronger in the defect area.

To conduct a complete evaluation of the defect distribution, the impact response (average amplitude) of each observed point is calculated, and the impact response is normalized (divided) according to the value at the same point on the observation line with no defects. Fig. 12 represents the distribution of the normalized impact response (NIR). Values of NIR for each track board are statistic, and it can be divided into three parts according to the magnification from results of numerical simulation. As defined above, for the escape of the mortar layer, the NIR should be greater than 40; for cracking and mud spillover in the support layer, the NIR should be 15–30; and for the no defect area, the NIR should be

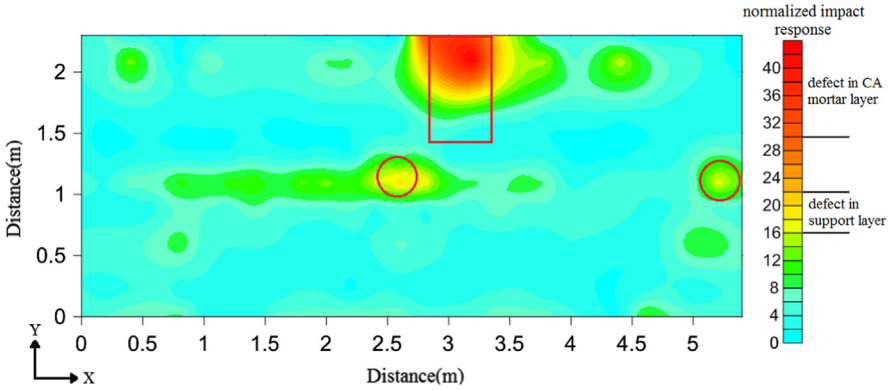

Fig. 13. Results of comprehensive evaluation.

1.0–10. However, with respect to the influence of noise and the coupling between layers, the NIR is divided into 3 ranks: NIR equal to or less than 10 is interpreted as signifying a no defect area; NIR greater than 40 is interpreted as signifying the escape of the mortar layer; and NIR of 20–30 is interpreted as signifying cracking and mud spillover in the support layer.

Considering the results from simulations, the final NIR values are expressed as a weighted average (W_r) of the three-directional results, in Eq. (1):

$$W_r = \frac{M_x}{M_x+M_y+M_z}(W_x) + \frac{M_y}{M_x+M_y+M_z}(W_y) + \frac{M_z}{M_x+M_y+M_z}(W_z) \quad (1)$$

where W_x, W_y, W_z are NIR values from filed tests in x, y, z direction, respectively; and M_x, M_y, M_z are average magnification of two types of defects from numerical simulation in x, y, z direction, respectively. The final results are shown in Fig. 13. Compared with Figs. 13 and 9, there are 9 measurement points in CA mortar layer defect area where 3 points at the boundary of the area and 4 measurement points in support layer defect area. Due to the impact source and the receivers have different sensitivity for defects, the impact source has higher sensitivity. And the response at the boundary of defects is affected by the position of the impact source. Anyway, the results are great affected by the type of impact. The distribution in x–y plane will shift to impact point. Compared with the presetting defects, it can be considered that this method can provide good results to identify the number of the defects and their locations and sizes.

5. Conclusion

A well-developed instrument is essential for a new NDT method applied to the investigation of the high-speed railway under-track structure. The integrating point-source/point-receiver scheme with a full-wavefield for defects imaging is developed. The image can expose the defect location in the high-speed railway under-track structure immediately after a series of impact-and-receive operations. The experimental result obtained from this system shows quite good agreement with the result simulated by the FEM method. The location and size of the defect can be clearly identified from the image. This full-wavefield imaging detection method therefore shows significant potential for detecting defects in the under-track structure of high-speed railways.

Acknowledgments

This work is financially supported by the National Natural Science Foundation of China (No. 11372180) and the Railway Ministry of Science and Technology Research and Development Program of China (No. 2013G004-A-1).

References

[1] Akira M. Structural dynamics for health monitoring. Nagaya, Japan: Sankeisha Co Ltd.; 2003. p. 77–96.
[2] Annigeri BS, Cleary MP. Surface integral finite element hybrid (SIFEH) method for fracture mechanics. Int J Numer Methods Eng 1984;20:869–85.
[3] Bocciolone M, Caprioli A, Cigada A, et al. A measurement system for quick rail inspection and effective track maintenance strategy. Mech Syst Signal Process 2007;21(3):1242–54.
[4] Chang YF, Wang CY, Hsieh H. Detecting cracks embedded in the concrete structure embedded in the concrete structure by reflection seismology method. NDT&E Int 2001;34:34–48.
[5] Che AL, Huang XC, Guo Q, Feng SK. Evaluation of mud-jack method filling effect of immersed tube tunnel using surface wave survey method. J Shanghai Jiaotong Univ 2011;45(5):648–58.
[6] Dalton RP, Cawley P, Lowe MJS. The potential of guided waves for monitoring large areas of metallic aircraft fuselage structure. J Nondestr Eval 2001;20:29–46.
[7] Farrar CR, Doebling SW. An overview of modal-based damage identification methods. Los Alamos, NM: Los Alamos National Laboratory; 1997.
[8] Fang YT. On China's high-speed railway technology. J Zhejiang Univ-Sci A (Appl Phys Eng) 2011;12(12):883–4.
[9] Feng, SK Che, AL, Wang, H, Huang, T . Study on the theory, method, and application of impact imaging method for grouting evaluation. In: Proceedings of the 11th SEGJ international symposium; geophysical for establishing sustainable secure socity. Yokohama; 18–21 November 2013.
[10] Keat WD, Erguven ME, Dwyer JF. Modeling of 3D mixed-mode fractures near planar biomaterial interfaces using surface integrals. Int J Numer Methods 1996;39:3679–703.
[11] Reithmaier Larry, Standard aircraft handbook for Mechanics and technicians, sixth edition, 1999, Mcgraw-Hill.
[12] L. Ljung and T. Glad, Modeling of Dynamic Systems, 1994, PTR Prentice Hall, Englewood cliffs, New Jersey 07632.
[13] Ling, HS . Research on the static and dynamic property of ballastless track based on fracture and damage mechanics. Doctoral thesis of Southwest Jiaotong University; 2009. p. 2–10.
[14] Liu C, Che AL, Feng SK. Propagation characteristics of elastic wave in layered medium and applications of impact imaging method. J Shanghai Jiaotong Univ 2013;18(3):1–7.
[15] Liu P, Tsai CD, Wu TT. Imaging of surface-breaking concrete cracks using transient elastic waves. NDT&E Int 1996;29:323.
[16] Love AEH. A treatise on mathematical theory of elasticity. New York: Dover Pubulications; 1944.
[17] Malhotra VM, Carino NJ. CRC handbook on nondestructive testing of concrete. Boca Raton, FL: CRC Press; 1991.
[18] Miller GF, Pursey H. On the partition of energy between elastic waves in a semi-infinite solid. Proc R Soc Lon Ser A. Math Phys Sci 1955;233(1192):55–69.
[19] Rose JL. A baseline and vision of ultrasonic guided wave inspection potential. J Press Vessel Technol Trans ASME 2002;124:273.
[20] Shaw MR, Millard SG, Molyneaux TCK. Location of steel reinforcement in concrete using ground penetrating radar and neural networks. NDT&E Int 2005;38(3):203–12.
[21] Shi HM. Research on recognition algorithm of track substructure defects based on vehicle dynamic responses. Int Fed Inf Process 2013;415:525–32.
[22] Tong JH, Liao ST, Lin CC. A new elastic-wave-based imaging method for scanning the defects inside the structure. IEEE Trans Ultrason Ferroelectr Freq Control 2007;54(1):128–37.